Supporting Information

Regulating DNA Self-Assembly Dynamics with Controlled Nucleation

Shuoxing Jiang[1], Nibedita Pal[2,†], Fan Hong[1], Nour Eddine Fahmi[1], Huiyu Hu[1], Matthew Vrbanac[1], Hao Yan[1,*], Nils G. Walter[2,*], Yan Liu[1,*]

[1]Center for Molecular Design and Biomimetics at the Biodesign Institute, and School of Molecular Sciences, Arizona State University, Tempe, AZ 85287, USA

[2]Single Molecule Analysis Group, Department of Chemistry, University of Michigan, Ann Arbor, MI 48109, USA

[†]Present address: Indian Institute of Science Education and Research (IISER) Tirupati, Tirupati 517507, Andhra Pradesh, India

Content

Page

S1 Data Analysis

S1.1 Thermal curves of the tile lattice: concentration dependence of T_m

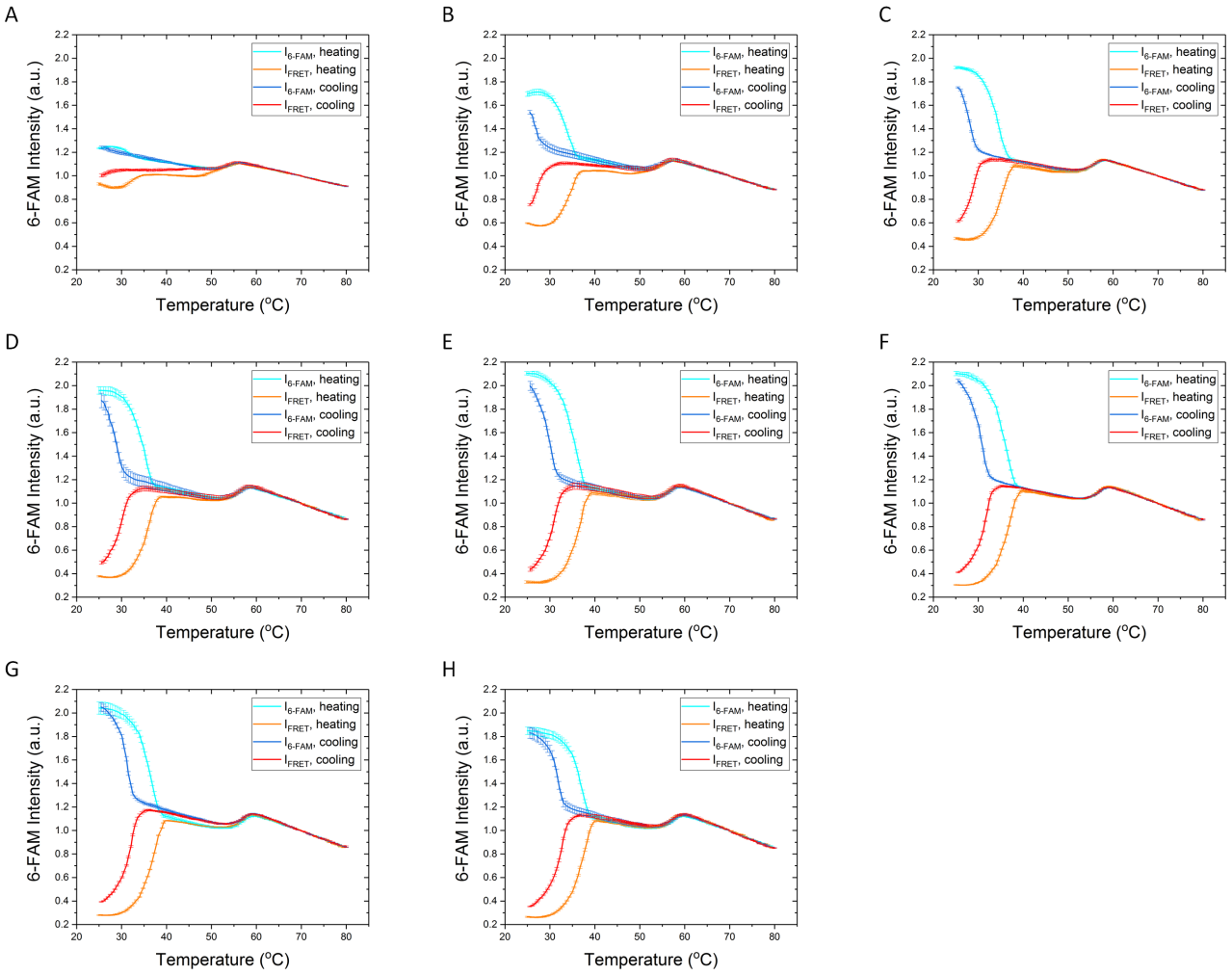

Figure S1. The cooling and heating curves (6-FAM fluorescence intensity *vs.* temperature) of the self-complementary tile lattices at different monomer tile concentrations. Tile concentrations are (A) 100 nM; (B) 200 nM; (C) 300 nM; (D) 400 nM; (E) 500 nM; (F) 600 nM; (G) 700 nM; (H) 800 nM. The transition at 50-60°C corresponds to the tile formation (*i.e.,* complete incorporation of the 6-FAM modified strand into the tile); the transition below 45°C corresponds to the growth of the lattice (*i.e.,* inter-tile binding through sticky end hybridization). $I_{6\text{-FAM}}$: 6-FAM intensity of the donor-only sample, I_{FRET}, 6-FAM intensity of the donor-acceptor dual labeled sample.

The fluorescence intensity difference of 6-FAM (ΔI) between the donor only ($I_{6\text{-FAM}}$) and donor/acceptor (I_{FRET}) samples at each temperature was calculated by the following equation:

$$\Delta I = I_{6-FAM} - I_{FRET} \qquad (1)$$

where $I_{6\text{-FAM}}$ and I_{FRET} are the fluorescence intensities of the donor 6-FAM in the absence and presence of the acceptor, respectively. ΔI was assumed to be proportional to the concentration of bound tiles. At each temperature, the growth of tiles onto the lattice reached equilibrium because of the slow temperature gradient. The melting temperature was then obtained by fitting the first derivative of ΔI *vs.* temperature with a Gaussian function:

$$f(T \mid T_m, w^2) = Y_0 + \frac{A}{w\sqrt{\pi/2}} e^{-2\left(\frac{T-T_m}{w}\right)^2} \qquad (2)$$

where T_m is the midpoint of transition temperature and w represents the width of the transition, which is ~0.849 of the full width of the peak at half maximum (FWHM). The concentration dependence of T_m was analyzed by the following equation, which assumes a two-state model,[1] to obtain standard enthalpy (ΔH°) and entropy (ΔS°) change for single tile attachment:

$$\frac{1}{T_m} = \frac{R\,ln(C_0/2)}{\Delta H^o} + \frac{\Delta S^o}{\Delta H^o} \qquad (3)$$

Table S1. Experimentally measured T_m of the tile lattice that increases with the tile concentration.

Concentration (nM)	T_m (°C)
100	31.9±0.1
200	33.8±0.1
300	34.4±0.1
400	35.0±0.1
500	35.6±0.1
600	35.8±0.1
700	36.3±0.1
800	36.8±0.1

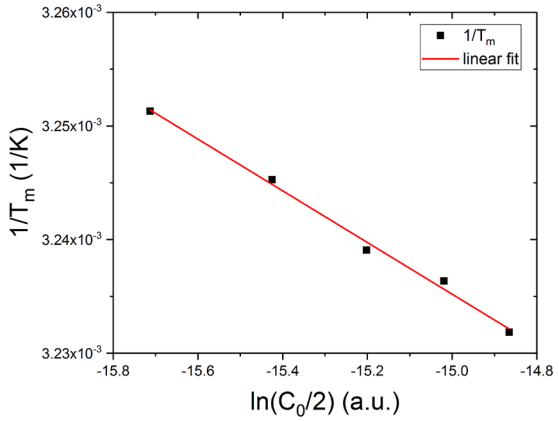

Figure S2. Linear fitting of the concentration-dependent T_m gives the standard enthalpy change (ΔH° = -87.4 ± 5.3 kcal/mol), entropy change (ΔS° = -0.252 ± 0.015 kcal/mol). Thus, the standard free energy change (ΔG°) for the attachment of a monomer tile can be calculated as -12.1 kcal/mol at 298 K. Data points for 300-700 nM were used for this plot. Data points for 100 and 200 nM were excluded due to the relatively weak transitions, and data point for 800 nM was not used due to detector signal saturation

Note: The thermodynamic parameters obtained here agree well with the values obtained from a previous study on the elementary steps in DNA tile-based self-assembly,[5] which gives ΔH° ranging from -85.2 to -95.1 kcal/mol, ΔS° ranging from -0.244 to -0.271 kcal/mol, and ΔG° ranging from -12.3 to -14.3 kcal/mol for bivalent tile attachment mediated by two sticky ends, 5-nt each. The small changes in thermodynamic parameters result from the weaker sticky ends (40% GC content) used in this study. The thermodynamic parameters are subsequently used to parameterize the kinetic model to predict the competition between different nucleation modes in this study.

S1.2 Thermal curves of the tile lattice: [Mg^{2+}] dependence of T_f

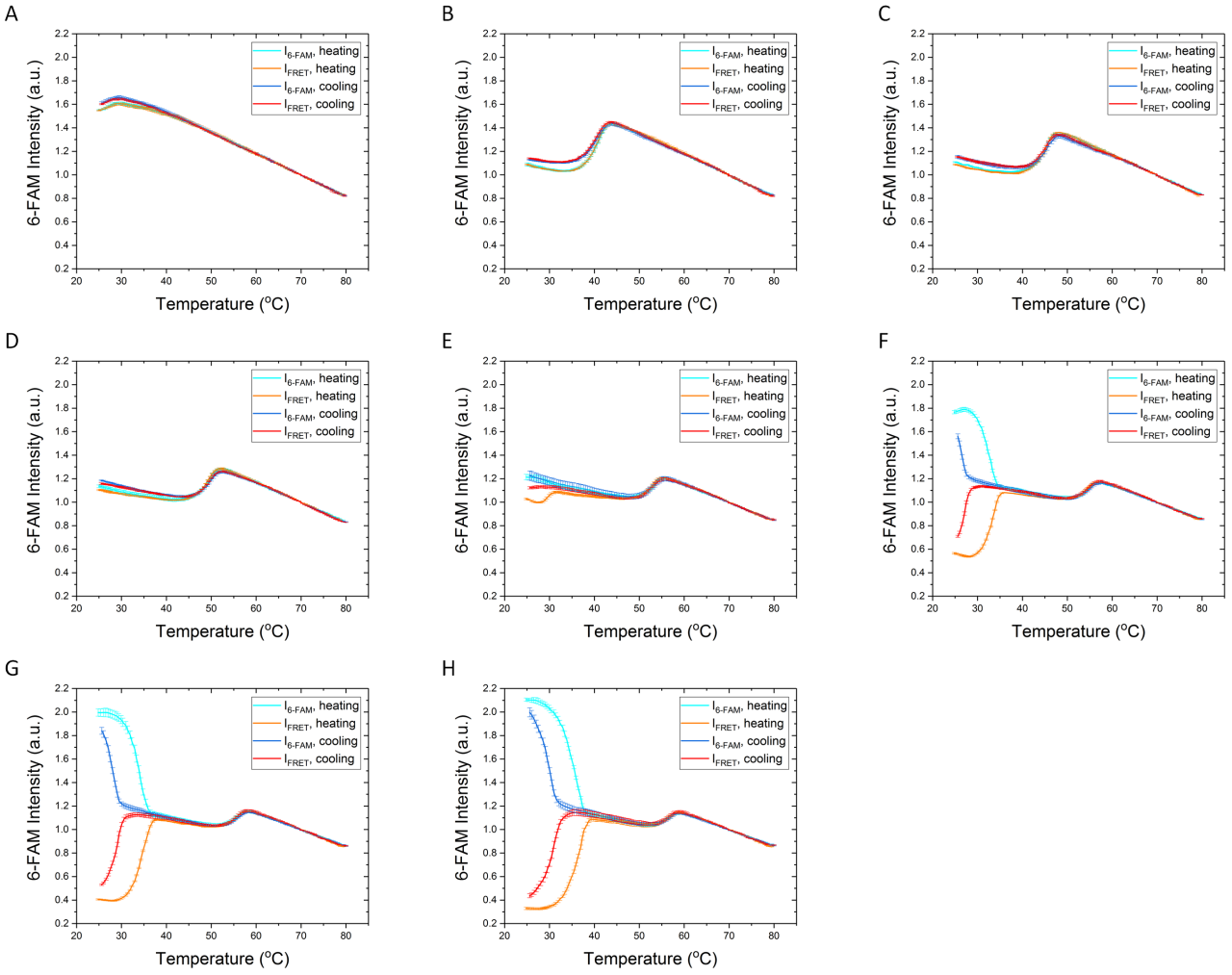

Figure S3. The cooling and heating curves (6-FAM fluorescence intensity *vs.* temperature) of the self-complementary tile lattices in 1×TAE buffer containing different [Mg^{2+}]. (A) 2.0 mM; (B) 2.5 mM; (C) 3.0 mM; (D) 4.0 mM; (E) 6.0 mM; (F) 8.0 mM; (G) 10.0 mM; (H) 12.5 mM. As [Mg^{2+}] decreases, both transitions of tile formation and tile growth shift to lower temperature regions. The transition of lattice growth no longer exists above 25°C when [Mg^{2+}] is below 3.0 mM, showing overlapping $I_{6\text{-FAM}}$ and I_{FRET} curves for both heating (cyan and orange) and cooling (blue and red) cycles. Thus, 2.5 mM [Mg^{2+}] was used to prepare monomer tile solution at room temperature. Considering the chelation ability of 2.0 mM EDTA in the buffer recipe, the effective [Mg^{2+}] is ~ 0.5 mM to maintain a stable monomeric tile at room temperature.

S1.3 Stability of the monomer tile

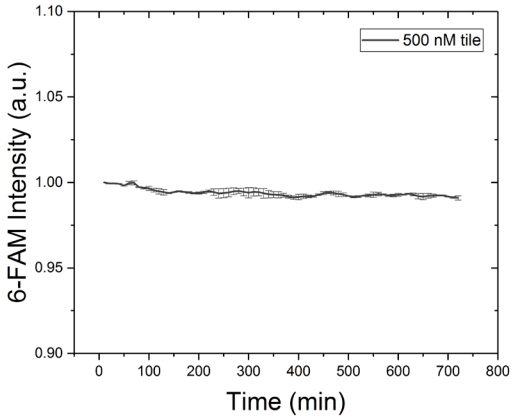

Figure S4. Stability test of the 500 nM monomer tile in 1×TAE buffer containing 2.5 mM Mg^{2+} at 26°C. The 6-FAM intensity remains stable over 12 hours except for a 1% signal decrease due to photobleaching of the 6-FAM reporter. Hence, the 500 nM monomer tile stock was held at 26°C to prevent spontaneous nucleation during the lengthy kinetic measurements.

S1.4 Thermal curves of seeded and facet nucleation

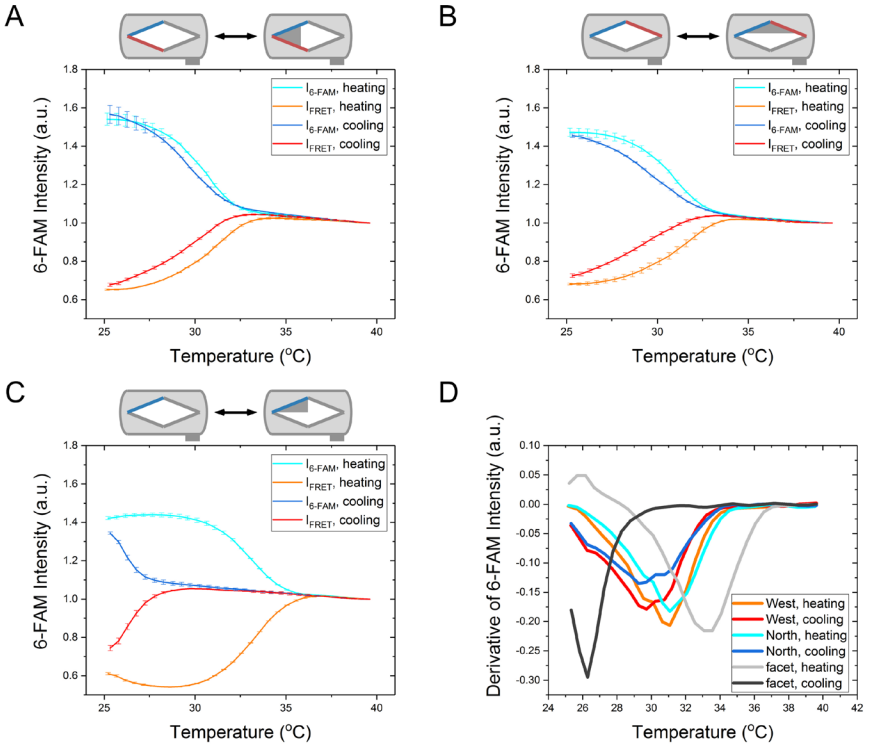

Figure S5. The cooling and heating curves (6-FAM intensity *vs.* temperature) of 100 nM self-complementary tile lattices in the presence of 4 nM nucleation seeds that present various growth frontiers measured from 25-40°C. (A) West frame presenting a bivalent binding site at the West corner; (B) North frame presenting a bivalent binding site at the North corner; (C) facet frame presenting monovalent binding sites along the NW edge. (D) The first derivative of the cooling and heating transition of the seeded and facet nucleation. The transition along the cooling curve represents the formation of the tile lattice (the midpoint of the transition is T_f), while the transition long the heating

curve represents the dissociation of tiles from the tile lattice (the midpoint of the transition is T_m). Comparing to unseeded nucleation of the same tile concentration (100 nM, Figure S1A) that only shows an incomplete growth transition down to 25°C, the presence of a bivalent seed significantly increases the T_f to ~30°C. The nucleation seed with a bivalent binding site facilitates nucleation more effectively than the facet frame with only monovalent binding sites, resulting in a ~4°C difference in the lattice formation temperature. In all cases, a hysteresis between the heating and cooling curves was observed. The presence of West or North frame reduces the hysteresis between the T_f and T_m to ~2°C, but cannot eliminate it.

S1.5 Kinetic curve normalization

The original fluorescent curves were processed by applying photobleaching correction and normalization to reflect the fractional yield of tile attachment. Although the protocol for kinetic measurement was optimized to minimize the effect of photobleaching, the 1800 s excitation time still results in ~2.5% reduction in the fluorescence intensity of the reporter fluorophore, 6-FAM (Figure S6). The effect of photobleaching was quantified by monitoring unseeded nucleation at 26°C, which is high enough to inhibit unseeded nucleation of 20 nM tiles. Then, the fluorescent curve was normalized to the initial fluorescent intensity at time 0 (I_0) and fitted by a linear function, which serves as the correction function for photobleaching. The normalization and correction were applied to all the other kinetic curves. To obtain the yield of tile attachment, the kinetic curves were normalized by the theoretical percentage of fluorescence enhancement when all the tiles are consumed by self-assembly. 40% fluorescence enhancement was adapted from the elementary tile attachment study[2] and applied to the normalization.

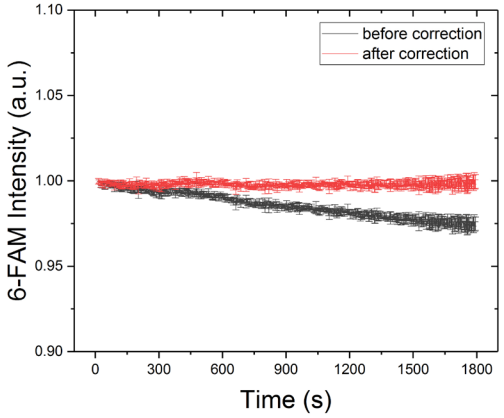

Figure S6. The baseline for photobleaching correction. The baseline was obtained by monitoring the kinetic curves of unseeded nucleation at 26°C, which was high enough to inhibit unseeded nucleation in solution. Photobleaching resulted in ~2.5 % reduction in the fluorescence intensity for the averaged kinetic curve of triplicate measurements. Fitting the kinetic curve with a linear function gave the slope of photobleaching as $-(1.394\pm0.009)\times10^{-5}$ s^{-1}, which was used to correct photobleaching for all the kinetic curves.

S2 Design of the DNA Origami Frame

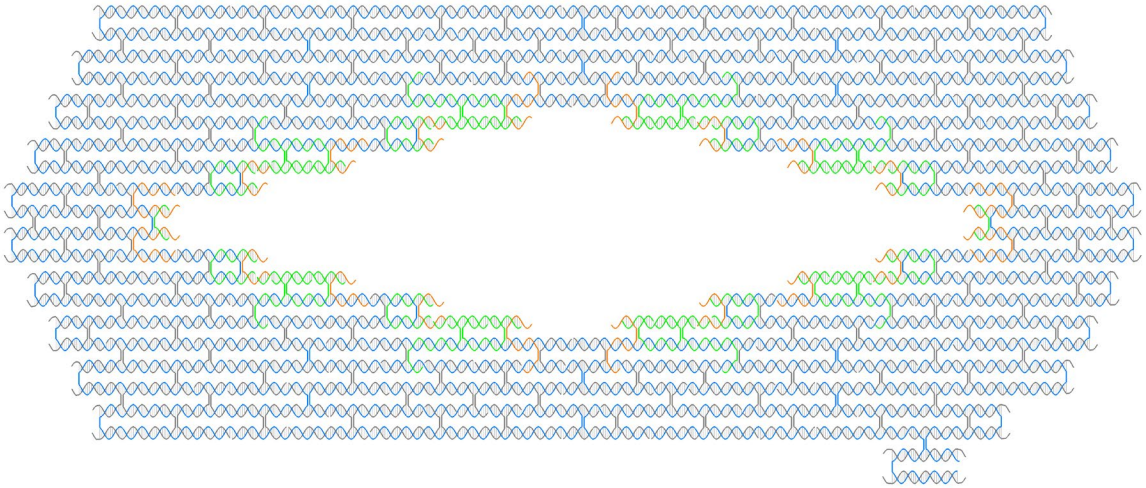

Figure S7. Detailed design of the DNA origami frame for kinetic measurements. The blue strand represents the M13mp18 scaffold. The interior edge is composed of staple strands carrying the sticky ends (orange) and the other staple strands holding the sticky ends in position (green). The rest of the staple strands (gray) fold the scaffold into the frame. The staple strands on the outer edges are extended by three thymine bases on both ends to avoid π-π stacking between origami frames. Sequences of the staple strands are listed in Table S6-8.

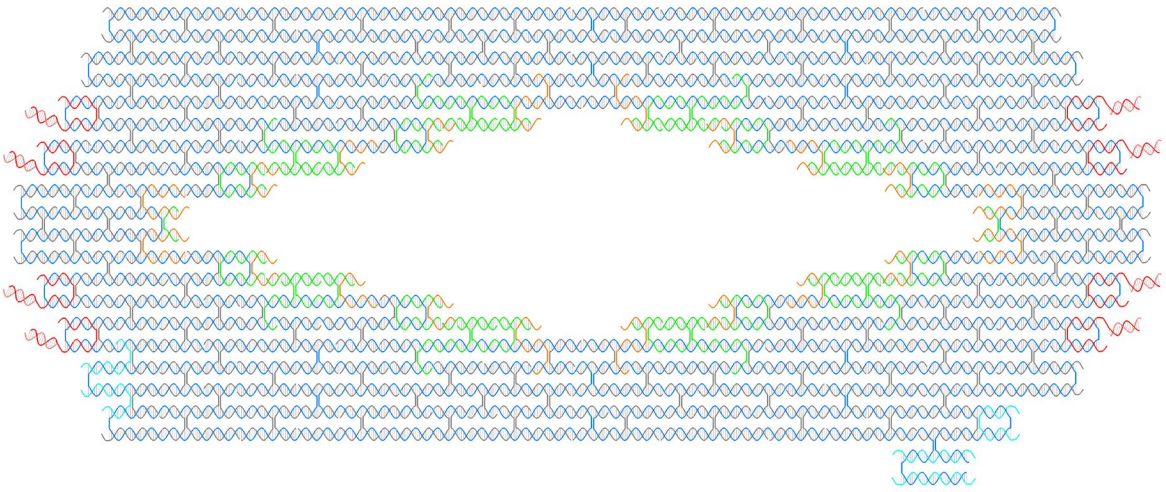

Figure S8. Detailed design of the DNA origami frame for single-molecule tile counting. The blue strand represents the M13mp18 scaffold. The interior edge is composed of staple strands carrying the sticky ends (orange) and staple strands holding the sticky ends in position (green). Eight positions (red) are extended for hybridizing with Atto647 labeled strand (pink) as the fluorescent marker. Five staple strands (cyan) are labeled with biotin for immobilization on the streptavidin-modified substrate surface. The rest of the staple strands (gray) fold the scaffold into the frame. The staple strands on the outer edges are extended by three thymine bases on both ends to avoid π-π stacking between origami frames. Sequences of the staple strands are listed in Table S6-9.

S3 Kinetic Simulation by Ordinary Differential Equation (ODE) Model

S3.1 Assumptions

The reversibility of the reaction depends on the number of sticky ends involved (for the same length and strength of the sticky ends). Tile attached by one bond is more likely to dissociate than the tile attached by two bonds under the experimental conditions in this study. To predict the competition between the three nucleation modes, we made the following assumptions:

1. The formation of a complex in which every tile is attached by two bonds is considered successful nucleation, after which the assembly proceeds into the growth stage.

2. The difference between the three modes of nucleation is the number of 1-bond attachment steps required to form a critical nucleus.

3. In the growth stage, the nucleus can transform free tile(s) to bound tile(s) by 2-bond attachment and grow larger.

$$\text{nucleus} + \text{tile}_{\text{free}} \underset{k_{2b,off}}{\overset{k_{2b,on}}{\rightleftharpoons}} \text{nucleus} + \text{tile}_{\text{bound}} \qquad (4)$$

4. No matter how large the lattice is, the thermodynamic and kinetic properties of an attached tile are exclusively determined by the number of sticky ends that are involved.

5. The joining or splitting of existing lattices are not considered contributors to lattice growth or dissociation in this model.

S3.2 Thermodynamic and kinetic parameter initialization

For the tile used in this study, the bivalent attachment (2-bond) thermodynamics was measured by the tile concentration-dependent melting curve. A loop penalty ($\Delta G_{Loop4}°$) is defined as the energy penalty to attach a tile through 2 bonds.[2] $\Delta G_{Loop4}°$ is defined as +3.0 kcal/mol. The free energy change for 1-bond attachment is calculated from 2-bond attachment as follows:

$$\Delta G^{o}_{1b} = (\Delta G^{o}_{2b} - \Delta G^{o}_{Loop4}) / 2 \qquad (5)$$

The rate constant of 2-bond attachment had been acquired from a previous study of single tile attachment.[2] The rate constant of 1-bond attachment was assumed to be equal to 2-bond attachment according to the assumption of kinetic tile assembly model (kTAM).[3-5]

Table S2. Thermodynamic and kinetic parameters used for the ODE modeling.

Number of bonds	ΔH° (kcal/mol)	ΔS° (kcal/mol)	ln(A·M·s)	E_a (kcal/mol)
1	/	/	26.7	7.6
2	-87.4	-0.252	26.7	7.6

S3.3 ODE set.

Table S3. Species selected for the ODE model.

Starting materials	Intermediates	Products
$\text{tile}_{\text{free}}$	dimer	$\text{tile}_{\text{bound}}$ (unseeded)
	trimer	
	unseeded nucleus	
facet	facet·tile	$\text{tile}_{\text{bound}}$ (facet)
	facet nucleus	
seed	/	$\text{tile}_{\text{bound}}$ (seeded)

A set of initial, intermediate, and product species (Table S3) are selected to depict the possible elementary reactions in the experimental system. The initial concentrations of the starting materials, including free monomer tile, facet, and seed, were initialized as 20.0, 6.4, and 0.8 nM, respectively. The interconversion between the above-mentioned species can be described by the following elementary reactions:

1. Unseeded nucleation and growth. Longer arrows indicate the thermodynamically preferred direction of the reaction under the modeling conditions.

$$\mathrm{tile_{free}} + \mathrm{tile_{free}} \underset{k_{1b,off}}{\overset{k_{1b,on}}{\rightleftharpoons}} \mathrm{dimer}$$

$$\mathrm{dimer} + \mathrm{tile_{free}} \underset{k_{1b,off}}{\overset{k_{1b,on}}{\rightleftharpoons}} \mathrm{trimer}$$

$$\mathrm{dimer} + \mathrm{dimer} \underset{k_{2b,off}}{\overset{k_{2b,on}}{\rightleftharpoons}} \mathrm{nucleus_{unseeded}}$$

$$\mathrm{trimer} + \mathrm{tile_{free}} \underset{k_{2b,off}}{\overset{k_{2b,on}}{\rightleftharpoons}} \mathrm{nucleus_{unseeded}}$$

$$\mathrm{nucleus_{unseeded}} + \mathrm{tile_{free}} \underset{k_{2b,off}}{\overset{k_{2b,on}}{\rightleftharpoons}} \mathrm{nucleus_{unseeded}} + \mathrm{tile_{bound}}$$

2. Facet nucleation and growth.

$$\mathrm{facet} + \mathrm{tile_{free}} \underset{k_{1b,off}}{\overset{k_{1b,on}}{\rightleftharpoons}} \mathrm{facet \cdot tile}$$

$$\mathrm{facet \cdot tile} + \mathrm{tile_{free}} \underset{k_{2b,off}}{\overset{k_{2b,on}}{\rightleftharpoons}} \mathrm{nucleus_{facet}}$$

$$\mathrm{facet} + \mathrm{dimer} \underset{k_{2b,off}}{\overset{k_{2b,on}}{\rightleftharpoons}} \mathrm{nucleus_{facet}}$$

$$\mathrm{nucleus_{facet}} + \mathrm{tile_{free}} \underset{k_{2b,off}}{\overset{k_{2b,on}}{\rightleftharpoons}} \mathrm{nucleus_{facet}} + \mathrm{tile_{bound}}$$

3. Seeded nucleation and growth.

$$\mathrm{nucleus_{seeded}} + \mathrm{tile_{free}} \underset{k_{2b,off}}{\overset{k_{2b,on}}{\rightleftharpoons}} \mathrm{nucleus_{seeded}} + \mathrm{tile_{bound}}$$

Some species such as $\mathrm{tile_{free}}$ and dimer are shared among the three nucleation modes. Thus, different nucleation types compete and inhibit each other through the consumption of these mutual species. The corresponding ordinary differential equations are simulated using MATLAB's stiff "ode23s" solver under conditions mimicking the experimental conditions.

S4 Additional AFM Images and Yield Quantification

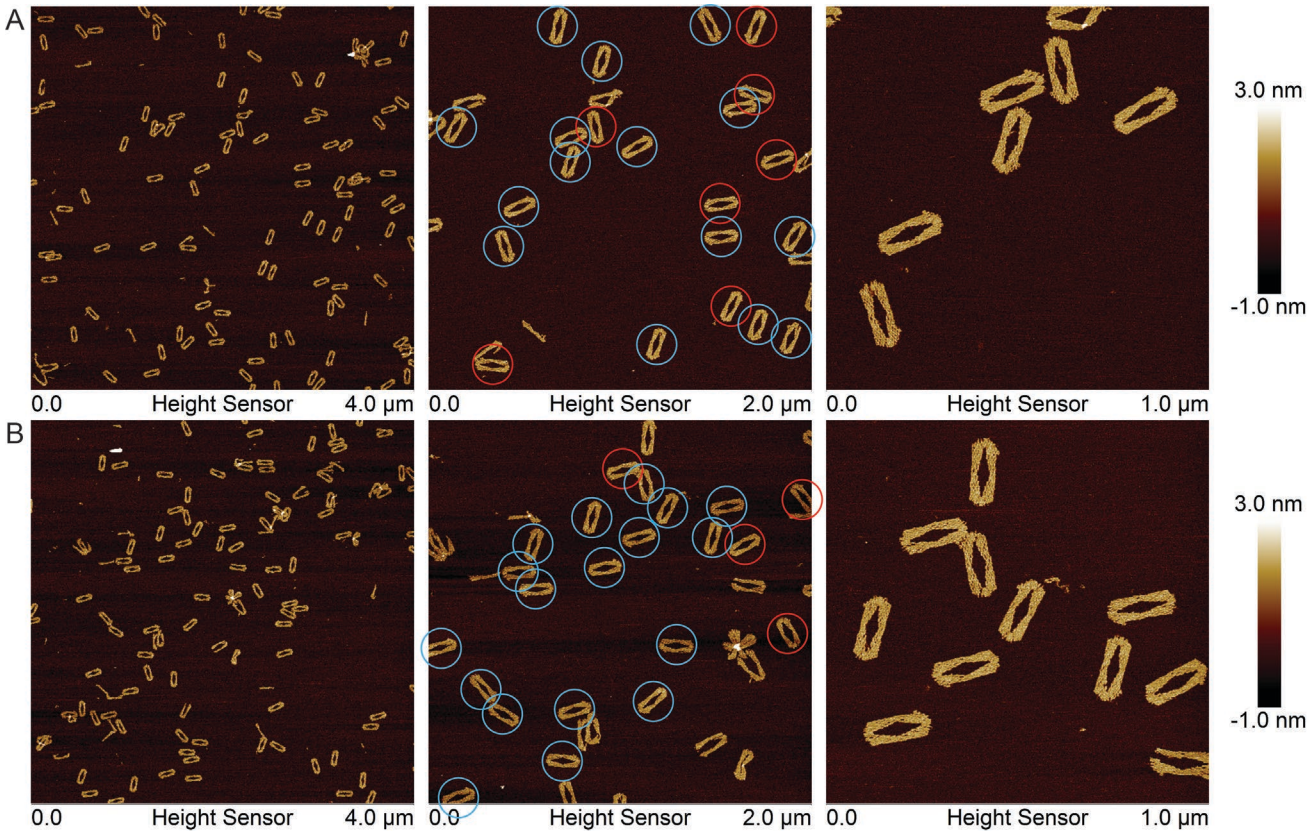

Figure S9. AFM characterization of the empty DNA origami frame. Scan size reduces from left to right. (A) West frame; (B) North frame. Monomeric origami frames were evenly distributed on the AFM substrate, suggesting the mono-dispersity of frames in solution. Some malformed origami frames were observed, which were majorly caused by the nicking of the M13mp18 scaffold strand. The malformed origami reduced the effective concentration of the frame. The asymmetric marker labeled at the bottom right of the origami frame allowed us to tell the direction of the origami frame landing on the substrate. Origami frames adopting face-up and face-down orientations were marked with red and blue circles, respectively. For the West frame, the ratio between face-up and face-down orientations is 7:15. For the North frame, the ratio is 4:18. The majority of the empty origami frames adopted the face-down orientation when depositing onto the mica surface (blue circle), suggesting that the curvature of the origami frame was in agreement with the curvature of the DAE-E tile used in this study.[6]

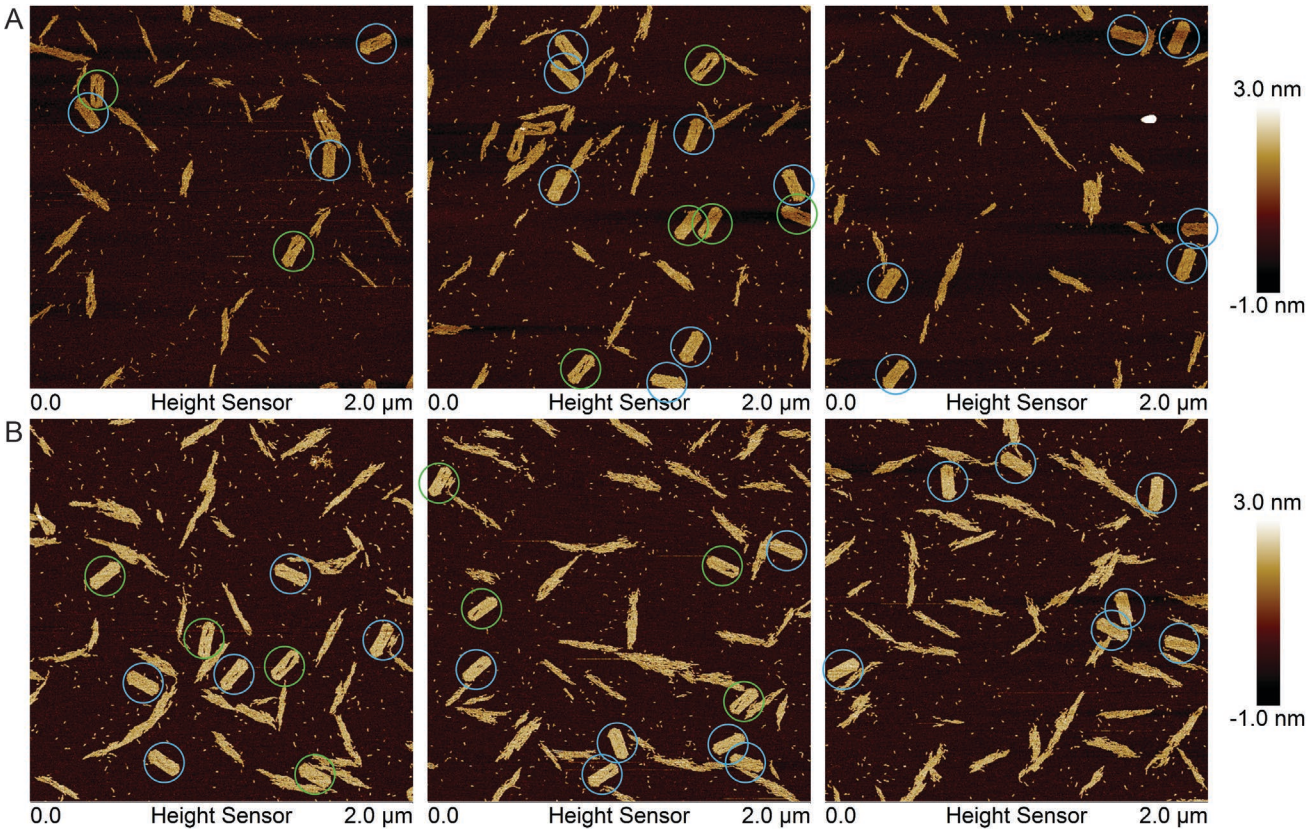

Figure S10. AFM characterization of the DNA origami frame filled by 2-fold DNA tiles (molar concentration ratio of the origami frame: tile = 1:50) at 22°C for 1 hr. (A) West frame. (B) North frame. Three non-overlapping scanning areas were shown for each sample. Partially filled and fully-filled frames were marked with green and blue circles, respectively. The majority of the well-formed frames were filled with > 90% yield with maximum 3 tiles missing. The missing tiles could be attributed to the reduced accessibility of the growth frontier when the growth was approaching the boundary of the template. Kinetic measurement suggested that 22°C did not favor unseeded nucleation in solution. However, mica substrate greatly promoted the heterogeneous nucleation of free tiles on its surface during 2 min sample preparation.[7] The lattice growth outside of the frame was mainly due to substrate surface-mediated nucleation during imaging.

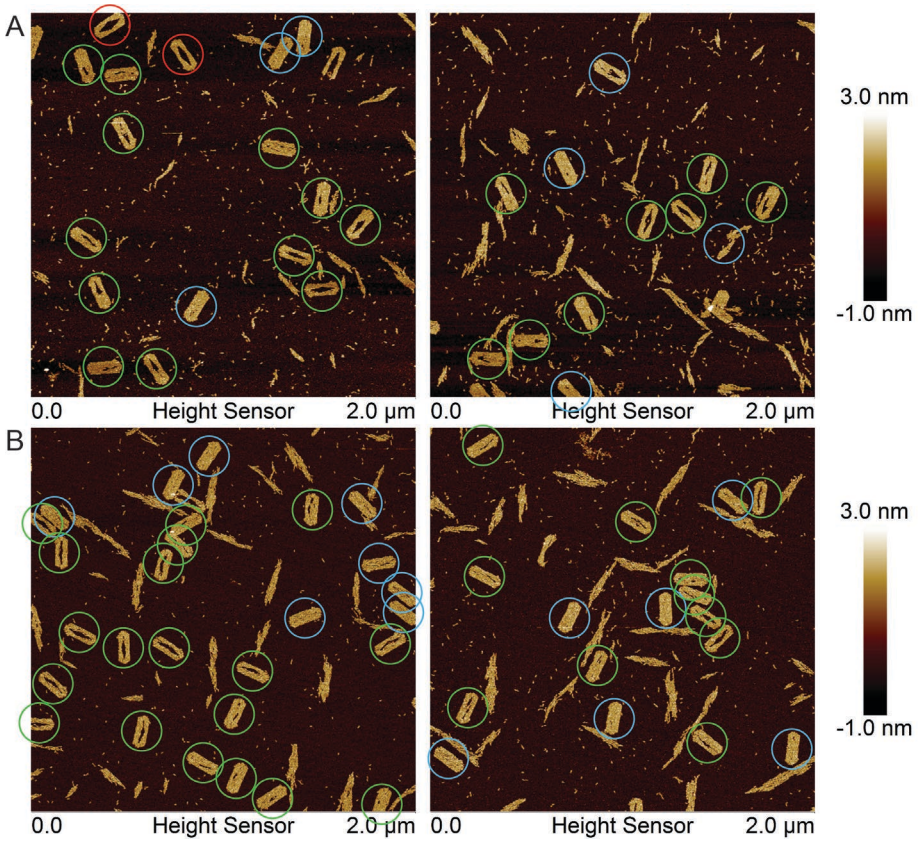

Figure S11. AFM characterization of the DNA origami frame filled by 1-fold DNA tiles (molar concentration ratio of the origami frame: tile = 1:25) at 22°C for 1 hr. (A) West frame. (B) North frame. Two different scanning areas were shown for each sample. Empty, partially filled, and fully-filled frames were marked with red, green, and blue circles, respectively. The average filling yield was approximately 60% for both frame designs. Again, the tile lattices outside the frame were mainly attributed to surface-mediated nucleation and growth during imaging.

S5 Stepwise Photobleaching Counting of Single-Fluorophore Labeled Tiles

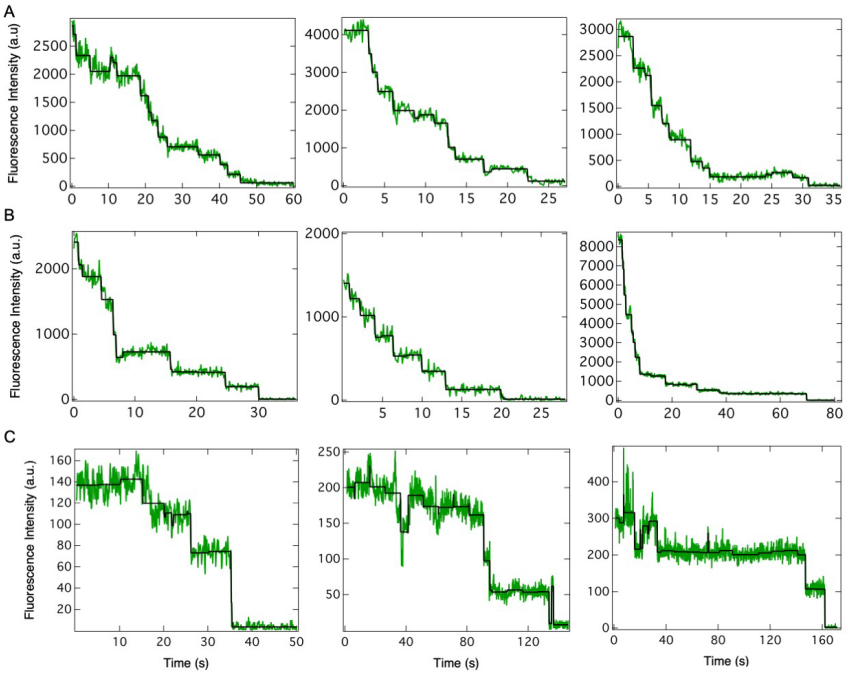

Figure S12. Representative single-tile stepwise photobleaching trajectories (green) of seeded W- (A), N- (B), and facet (C) frames with respective detected steps (black).

Table S4. Quantitative analysis of single-tile stepwise photobleaching experiment.

Frame	Number of origami frame investigated	Average number of tiles nucleated in a frame	Maximum number of tiles nucleated in a frame	Minimum number of tiles nucleated in a frame
W	70	13 ± 7	32	4
N	72	12 ± 6	32	5
facet	10	4 ± 2	8	2

[#] The error bars are given as the standard deviation of all the data.

S6 Sequence

Table S5. Sequences of the oligos composing the DNA tile.

Name	Sequence
tile-1	CTAGATCCTGACAATACAACCGCCATTCCTGAGACGA
tile-1-3'FAM	CTAGATCCTGACAATACAACCGCCATTCCTGAGACGA/36-FAM/
tile-2	TCAGTTCGTCTCACCGTAACCAGGTA
tile-3	TGTATTGTCACCGACAGCAGGTCCAGGCAGTGGAATGGCGGT
tile-3-5'Cy3	/5Cy3/TGTATTGTCACCGACAGCAGGTCCAGGCAGTGGAATGGCGGT
tile-4	ACTGAGTCGGAGTGGATCTAGTACCT
tile-4-5'TMR	/56-TAMN/ACTGAGTCGGAGTGGATCTAGTACCT
tile-5	GGTTACGGACTGCCTGGACCTGCTGTCGGACTCCGAC

Table S6. Sequences of the staple strands (gray-colored in Figure S7) composing the DNA origami frame.

Name	Sequence
Frame4Turn_core2	ATTAACCGTTGTAGGCCGATTAAAGGGATTTTAGACAGGGCTAGGGCGCTGG
Frame4Turn_core3	CAAGTGTAGCGGTTTAGAGCTTGACGGGGAAAGCCGGCGTCCACTATTAAAG
Frame4Turn_core4	CCCCCGATCACGCTGCGCGTAACCCGGGAGCT
Frame4Turn_core5	AGAACTCAAGCACGTATAACGTGCTTTCCTCGTTAGAATCAGAGACCACACC
Frame4Turn_core6	CGCCGCGCTTAATGCGCCGCCGTAAAGCACTAAATC
Frame4Turn_core7	GGGGTCGAGGTGCTACAGGGCGCGTACTATGGACTGTTGGGA
Frame4Turn_core8	AGGGCGATCGGCAATTCCACACAACATACGAGCAAGTTTTTT
Frame4Turn_core9	GAAATTGTTATCCGCTCATGCGGGCCTCTTC
Frame4Turn_core10	GCTATTACGCCAGTGGTGCCGGAAACCAGGC
Frame4Turn_core11	AGGGGGATCATGGTCATAGCTGTTCTCACATT
Frame4Turn_core12	CTGCCCGCAGCTCGAATTCGTAATGTGCTGCAAGGCGATT
Frame4Turn_core13	AAGTTGGGTAACGCCGATCCCCGGGTACCGTTTCCAG
Frame4Turn_core14	GCCAGCTGCAGGTCGACTCTAGAGAGGGTTTT
Frame4Turn_core15	GCATCTGCCAGTTTGACGACGTTGTAAAA
Frame4Turn_core16	CGACGGCCAGCAAATATTTGGCGCATCGTAACCGT
Frame4Turn_core17	CGGAGAGGGAACGGTAATCGTAAAACTAGCATGTTAAATCAG
Frame4Turn_core18	AACCCGTCTTAACCAATAGGAACGCCATCAAAAAAAACAAGA
Frame4Turn_core19	GAGTCTGGAGCTAATTCGCGTCTGGCCTTCCTTATCGCGTTT
Frame4Turn_core20	TAATTCGAGCTTCCATATAACAGTTGATTCCCCATTGCCTGA
Frame4Turn_core21	GGTGTCTGGAAGTTTCATTCAAAGCGAACCAGACCG
Frame4Turn_core22	GAAGCAAAAGCGGATTGCATCAAAAAGATTAAGAGGAAGCCCGAATTTTGCAA
Frame4Turn_core23	AGAAGCAACTCCAACAGGTCAGGAGTTTTAAA
Frame4Turn_core24	TTTGGATGGCTTAGAGCTTAATTGCTGAATATAATGCTGTAGCTCAACATTTAGAGAG
Frame4Turn_core25	TACCTTTAATTGCTCCTTCAAAAATCAGGTCTTTACCCTGACTATAGCGTCC
Frame4Turn_core26	CCATAAATTTGATAAGAGGTCATTTTTGCTTT
Frame4Turn_core28	ATCGGCAAAATCCCTTATAAATCAAAACGTCAAAGGGCGAAAAAAGGGAG

Frame4Turn_core29	GGAACCCTAACCGTCTATCAGGGCGATGGCCCACTGATGGTGGTTCCGAA
Frame4Turn_core30	TTGCAGCACCTGGGGTGCCTAATGAGTGAGCTAATCCTGTGT
Frame4Turn_core31	TTGCATGCCTGCATTAATGAATCGGCCAACGCAAAGGGTG
Frame4Turn_core32	AAACGTTAAGCCCCAAAAACAGGAAGATTGTATAAGTGCCAAGC
Frame4Turn_core33	ATCAGAAAATATTTTGTTAAAATTCGCATTAAATTTTTGTCAATCATA
Frame4Turn_core34	CAATGCCTGAGTAATGCGGAGACAGTCAAATCACCATCAATAGGTTGATA
Frame4Turn_core35	TGTACCCCTGATATTCAACCGTTCTTTAGAACCCTCATATATTTTAAATG
Frame4Turn_core36	GAATCGATGTAGCTATTTTTGAGATTTTGCGGGAGAAGCC
Frame4Turn_core37	CCTCAGAGCATAATAGTTTGACCATTAGATACATTTCGCTAAAGTAC
Frame4Turn_core38	TATGCAACAAATGGTCAATAACCTGAAAAGGTGGCATCAATTCTACAATAAAG
Frame4Turn_core39	AACGTGGACTCCAAGAATAGCCCGAGATAGGGTTGAGTGTTGTTCCAGTTTTT
Frame4Turn_core40	AAAATCCTGTTTACGTGAACCATCACCCAAATCCGGAAGCAT
Frame4Turn_core41	AAAGTGTAAAGAGCGGTCCACGCTGGTTTGCCCCAGCAGGCG
Frame4Turn_core42	AATTGCGTGCTGATTGCCCTTCACCGCCTGGCCCTGAGAGAG
Frame4Turn_core43	TCGGGAAAGTTTTTCTTTTCACCAGTGAGACGGGCAACATGCGCTCA
Frame4Turn_core44	GCGGTTTGCGTATTGGGCGCCAGGGTGCCTGTCGT
Frame4Turn_core45	AGAAAGGCTGTAGGTAAAGATTCAGCGGGGAGAG
Frame4Turn_core46	TTTATTTCAACGCAAGGATAAAAATTTAGCTGATAAATTAATGC
Frame4Turn_core47	CCCTGTAATACGATCTACAAAGGCTATCAGGTAATTCTGCGA
Frame4Turn_core48	ACGAGTAGATTAGCTAAATCGGTTGTACCAAAAACATTATGA
Frame4Turn_core49	TTTTAATTCTGTCCAGACGACGACAATAAACAACATGTTCGTAATAAGAGAAT
Frame4Turn_core50	ATATGCGTAGGCATTTTCGAGCCAAGCTAATGCAGAACGCGCCTGTTTAT
Frame4Turn_core51	CAACAATAGATAAGTCACAACGCCAACATGTAATTTAGGCAGTATACAAA
Frame4Turn_core52	CGCCATATTTACTGAACAAGAAAAATAATATCCCATCCTAAT
Frame4Turn_core53	TTACGAGCATGCTTAAATCAAGATTAGTTGCTAATTGAGAAT
Frame4Turn_core54	ACGCTAACTCCCGACTTGCGGGAGGTTTTGAAGCTAGAAACC
Frame4Turn_core55	AATCAATAATCGGCTGTCTTTCCTTATCATTCCAGGCGTTTT
Frame4Turn_core56	GAACGCGAAGAACGGGTATTAAACCAAGTACCGCACTCAAGAAGGCT
Frame4Turn_core57	TCAGATATTCGAGAACAAGCAAGCCGTTTTTATTT
Frame4Turn_core58	TCATCGTAGGCATAATCAAAATCACCGCGTTTGC
Frame4Turn_core59	CCGACTTGCATTTTCGGTCATAGCCCCCTTATTAGGAACCAGAGCCACCA
Frame4Turn_core60	CCGGAACCGCCTCCCTCAGAGCCGCCAGCGCGTTTTCATCGGAGCCATTT
Frame4Turn_core61	CCTTTAGCGTCAGACTGTACCCTCAGAACCGCCACCCTCAGAGC
Frame4Turn_core62	CACCACCCTCAGAGCCTCAGTAGCGACAGAATATTACCAT
Frame4Turn_core63	CAGCACCGTAAGCCACCAGAACCACCACCAGAGCCGCCGCCA
Frame4Turn_core64	GCATTGACAGGGGTCAGTGCCTTGAGTAACAGCCATCGATAG
Frame4Turn_core65	ACCTATTAAGTGTACTGGTAATAAGTTTTAACGGAGGTTGAGGCAGGTCA
Frame4Turn_core66	GACGATTGGCCTTGATATTCACAAACCTTTTGATGATACAGGTTCTGAAA
Frame4Turn_core67	GCGTCATACATGGAAATAAATCCTCATTAAAGCCAGAATGGAAAGCGCAGTTT
Frame4Turn_core68	TTTTTAAATAAGAATAAACACCGGAAAAGGTAAAGTTT

Frame4Turn_core69	ATAAAGTACCGACAATCATAATTACTAGAAAAAGCCTGTACCTAAATTTAAT
Frame4Turn_core70	AGCGAACCGAGCGTCTTTCCAGAGGACGGGAG
Frame4Turn_core71	CAGGGAAGCGCATTACCTAATTTGCCAGTTATATTCTAA
Frame4Turn_core72	TATCCGGCAAAATAAACAGCCAGAGAATAACATAAAAA
Frame4Turn_core73	TTTACAGATATTATTTATCCCAATCAAGCAAA
Frame4Turn_core74	CATCTTTTAATCATTACCGCGCCCAATAGCCAAATAAGAA
Frame4Turn_core75	TTTACCAGGAGCCAGCAAAATCACCAGTAGCACCCAAGTTTG
Frame4Turn_core76	GAGGGTTGATATATATTAAGAGGCTGAGACTCCTCAAGAACCGTTCCAGTAA
Frame4Turn_core77	TAACCTCCTTAATTTCATCTTCTGTTAGTATC
Frame4Turn_core78	TTCTTACCAGTATAAAGCAGAAAACTTTTTCAAATA
Frame4Turn_core79	CAAAGAACGCGCAACGCTCAACAGTAGGGCTTATTTTGCACC
Frame4Turn_core80	CAGCTACAATTAATTGAGCGCTAATATCAGAGAATCGCAAGA
Frame4Turn_core81	AAAGTCAGAGGGTTTATCCTGAATCTTACCA
Frame4Turn_core82	ACGATTTTTTGAAATTATTCATTAAAGGTGAATTATTGAGGGAG
Frame4Turn_core83	GGGAATTACGCCAAAGACAAAAGGGCGACATTCAACCGATCACCGTCA
Frame4Turn_core84	TAGCAAGGTTATTTTGTCACAATCAATAGAAAATAAACGTAGA
Frame4Turn_core85	ACGGAATAAGTCCGGAAACGTCACCAATGAAATGCCCGTATA
Frame4Turn_core86	AACAGTTAATGAGTACCGCCACCCTCAGAACCCAAAGACACC
Frame4Turn_core87	ACCGTACTCAGGAGGTTTCCCCCTGCCTATTTCGGA
Frame4Turn_core88	CATGAAAGAGTATAGCCCGGAATAGGATAGCA
Frame4Turn_core89	TTTTCTCTGAATTTGAAGGATTAGGATTAGCGGGGTTT
Frame4Turn_core90	TAGTGAATGACCGTGTGATAAATAAGGCGTTT
Frame4Turn_core91	GGTTTGAAATACCTTATCAAAATCATAGGTCTGAGAGACAAATCGTCGCTAT
Frame4Turn_core92	TATTTTAGGGCTTAGGTTGGGTTATATAACTATATGTAAATGCTAATGGAAA
Frame4Turn_core93	AATAATAAGAGCAAGAAAGAACACCCTGAAC
Frame4Turn_core94	TCAAAAATGAAAACAAAGTTACCAGAAGG
Frame4Turn_core95	AAACCGAGGAAACGCAAAATATTGACGGTTTAACG
Frame4Turn_core96	TTTCAACAGAACCGCCACCCTCAGAGCCACCACCCTCATTTTCAGGGTGTATC
Frame4Turn_core97	GTCTTTCCAGGAACCCATGTACCGTAACACTGAGTAAGTGCCGTCGA
Frame4Turn_core98	TTTTTTTGCTCAGTACCAGGCGGATTTCGTCA
Frame4Turn_core99	GCGTAGATTTTCAGGTTTACTTAGAATCCTTGAAAAGAGTCAA
Frame4Turn_core100	CATCGGGAATAACCTTGCTTCTGTTACCTTTT
Frame4Turn_core101	CATTTGAATTACCTTTTTTGATGCAAATCCAGATAACC
Frame4Turn_core102	CACAAGAATTGAGCATTTAACAATTT
Frame4Turn_core103	TTACCTGAAAAACAAAATTAATTATTAAGCCC
Frame4Turn_core104	AAATACATACATAAAGGCTAAAGGAATTGCGAAAAAAGGCT
Frame4Turn_core105	GAGAATAGAAAGGAACAATGGCAACATATAA
Frame4Turn_core106	AAGAAACGGCCACCCTCAGTTTCAGCGGAGT
Frame4Turn_core107	AGCCCAATAGACGTTAGTAAATGAGTTGCGCC
Frame4Turn_core108	CCAGTACACCTCATAGTTAGCGTAATATATTCGGTCG

Frame4Turn_core109	ACAGAGGCCAACAACCATCGCCCACGCATAACCGACGATCTAAAGTTTTGTC
Frame4Turn_core110	GATACCGATAATTTTCTGTATGGGATTTTGCTTAAACAGCTT
Frame4Turn_core111	CGGATTCGCCTTAAATCAATATATGTGAGTGAGAAACAATAA
Frame4Turn_core112	TAATTAATTTTCCACGTCAGATGAATATACAGTAACAGTCCTGATTG
Frame4Turn_core113	AAAAGTTTGTTAGAACCTACCATAAAGAAATT
Frame4Turn_core114	AGAAGGAGCGGAATTAAATTCATCAATATAATACCTTTTA
Frame4Turn_core115	GACAATGATTTGAGGACTAAAGACAAATACGTAATGCCAC
Frame4Turn_core116	CTGAGGCTTGCAGCCTCAGCAGCGAAAGAAATACACT
Frame4Turn_core117	GCAAAAGCAGCATCGGAACGAGGGTAGCAACGGCT
Frame4Turn_core118	TTTGGATTATACTTCTGAATAATGGAAGGGAGTAACA
Frame4Turn_core119	TATTTTTGATAGCCCTAAAACATCTCAAATAT
Frame4Turn_core120	GCTGAACCGCCATTAAAAATACCGAACGAACCACCAG
Frame4Turn_core121	CAGAAGATAGAACCCTTCTGACCTGAAAGCGTAAGTCCATCACGCAA
Frame4Turn_core122	ACAGAGATAAAACAGAGGTGAGGCCACGCTGAGAGCCAGC
Frame4Turn_core123	AATACTGCGGAATCGTCAGTTGGGAAGAAAAATCTACGTTAATAAAACACCA
Frame4Turn_core124	GAACGAGTAGTAAATTGGGCTTGAGATGGCTGACCTT
Frame4Turn_core125	AGGCTGGTTTAATTTCAACTTTAACTGGCT
Frame4Turn_core126	CATTATACCAGTCAGGACTAAATATTCATTGAATGAGAATGA
Frame4Turn_core127	AAAGCGCCATATTACCGCCAGCCACTACATTT
Frame4Turn_core128	AAAGGGACATTAGTAATAACATCACTTGCCTGACCAGTAATA
Frame4Turn_core129	AAACAGGAGCAATACTTCTTTGATTCTGGCCA
Frame4Turn_core130	GCCAGAATCCGAGTAAAAGAGTCTGAATACGTGGCACAGACAA
Frame4Turn_core131	GCTGCGCATTGCTTTGACGAACTATCGGCCTT
Frame4Turn_core132	GCTGGTAATATCCAGAACAATTCGCCATTCAG
Frame4Turn_core133	CTTTCATCAACATGACGACGATAAAAACCAA
Frame4Turn_core134	AATAGCGAGAGGCAGACTTCAAAGTAGCCAG
Frame4Turn_core135	ACAGGTAGAAATTGCCAGAGGGGGTAATAGTACAACATTATT
Frame4Turn_core136	TAACGGAAAAATGTTTAGACTGGATTATAGTC
Frame4Turn_core137	CCAAAAGGTAACCCTCGTTTACCATAAATGTGAGCGAGTAAC
Frame4Turn_core138	TTTAGAGGACAGATGAACGGTGTACAGACCAAGGGAACCGAACTGAAAGTACAA
Frame4Turn_core139	AAAACACTTGTATCATCGCCTGACAGACGGTCAATCATAGGCGCAT
Frame4Turn_core140	TTATCATTATAGATAATACATTTGTTAGGAGCACTAACAAATCACCTT
Frame4Turn_core141	CAAACCCTGTTATCTAAAATATCTAGGATTTAGAAGTATTTTAATTTT
Frame4Turn_core142	CGGAGATTCATCTTTGACCCCCAGCGATTATACCATTT
Frame4Turn_core143	TTTGTATTAAATCCTTTGCCCGAACGTTAAGACTTTA
Frame4Turn_core144	CAAACAAAAGGAATTGAGGAAGCAATCAATATCTGGTCAGTTGGCAAATTT
Frame4Turn_core145	CATCAAGATAGCCGGAACGAGGCGTAAATTGTGTCGAAATCGAAAGAG
Frame4Turn_core146	TATTCATTACCCAAATGGCTTGCCCTGACGAGAAACGAAC
Frame4Turn_core147	TTTTCAACAGTTGATTCGACAACTCTTT
Frame4Turn_core148	TTTAGCGCGAAACACCAACTTTGAATTT

Table S7. Sequences of the adaptor staple strands (green-colored in Figure S7) composing the DNA origami frame.

Name	Sequence
Frame4Turn_Adap1	TCCCTGATTTAAGGTCCAGCCAGCTTTCCGGCACCGCTTCCTGGCGAA
Frame4Turn_Adap2	CTCATTTTGGATTCTCCGTGGGAACAAACGGCGGATGTAGCAGGCGTCT
Frame4Turn_Adap3	AATTAACTCAATGAAATAGCAATAGCTATCTTACCTCCGGCTTCATTG
Frame4Turn_Adap4	AATTGATGCTCACAAGACTCCTTATTACGCAGTATGTTAGCTCATATGG
Frame4Turn_Adap5	TCCCACGCCAATCCGAAGCCCTTTTTAAGAAAAGAGCACGAT
Frame4Turn_Adap6	GCCGGAGGATTGGCGTGGGAATCGTGCTTCTGTCTC
Frame4Turn_Adap7	TATACCACCATTGCTTTCGAGGTGAATTTCTAAACAAC
Frame4Turn_Adap8	CGTTGAAGAAACAAACATCAAGGCAAAAGAAGATGATTATACGTC
Frame4Turn_Adap9	CAGTACAGATTGCTTTGAATACCGTTCTTGGGCGTA
Frame4Turn_Adap10	AGTCAGCTTGCTACAAGTTACAAAATCGCGCAGATTTGTTTG
Frame4Turn_Adap11	AAGAACGTAGCAAGCTGACTCAAACAAAATACATTC
Frame4Turn_Adap12	AGCCTGGTTATCAGATGATGGCTCATCATATTCCTGATTCAATAC
Frame4Turn_Adap13	CGTCAGTTCGCCTGCAACAGTGCGGTCAGTATTAACACGTAAAAT
Frame4Turn_Adap14	TGTGAGTTCTCAACATTCACCAGTCACACGAGTAGA
Frame4Turn_Adap15	GTCAGAACATGGATTATTTACATTGGCAGGAAGCACGTATCG
Frame4Turn_Adap16	CAGTGTAGGTTCTGACCGATACGTGCTTCGTTGAGA
Frame4Turn_Adap17	CTCCGTTTCGCTCATGGAAATACTTGCAACAGGAAAAAAATATCG
Frame4Turn_Adap18	TAGCACTGTCGGCCTCAGGAAGATCGCACTCATTCCATCCTC
Frame4Turn_Adap19	AAGAAGTTGATTCATCAGTTGAGAAGCGAGTCTCTGGA
Frame4Turn_Adap20	CGGAAACCCAGTGCTAGAGGATGGAATGACCTTAAA
Frame4Turn_Adap21	CCATAGACGACTAGCC
Frame4Turn_Adap22	CTGAGCGACCAAAAGAACTGGCATGATTATATTGGGAAGTTA
Frame4Turn_Adap23	TTGATACTCCTGTTTGACCGTAATGGGATAGGTCGTACGGGT
Frame4Turn_Adap24	GTCAACCCTTGAAAATCTCCAAAATAATAATTTTTTCACGGGATAAC
Frame4Turn_Adap25	GGCATATCTCGCTCAGTAACTTCCCAATATGTGAGC
Frame4Turn_Adap26	GCGGATACTGTATCGGTTTATCAGCTTGCACTAGATCTTGCG
Frame4Turn_Adap27	GCACTACGTTCCATTAAACGGGTATTTTTCATGAGGAAGTAGCTTAT
Frame4Turn_Adap28	GTGGGAGAGTATCCGCCGCAAGATCTAGTGCAATGG
Frame4Turn_Adap29	GAGATGCAGGAGAAGA
Frame4Turn_Adap30	CTCCCAACTCATTCAGTGAATAACAACGTAACAAAGCTGATCGTTAA
Frame4Turn_Adap31	AAATTTCGAAAACTTTAGGAATACCACATTCAACTTGAGGGC
Frame4Turn_Adap32	ACTCGCTGTTTTCGAAATTTGCCCTCAAGCGCGAGA
Frame4Turn_Adap33	TTGTTAGAAGAGCAACACTATCAAATTACGAGGCATAGTCTAGCGCA
Frame4Turn_Adap34	TGCTACAACAGGAGTATCAAACCCGTACAAAGGGAA

Table S8. Sequences of the staple strands (orange-colored in Figure S7) carrying the sticky ends, *b* stands for the blunt version of the staple, *stop* stands for stopper sticky ends used for the termination of tile assembly within frames. Different combinations were used to assign stick ends in a user-defined manner.

Name	Sequence
NW-1	ACTGAGGCTAGTCAGAGCCGTCATTGCGGAACAAAGAAACCACC
NW-2	ACTGAGTATTGAACCAGGCTTACGCCC
NW-3	ACTGAGAATGTATGGCGAATTATTCATTTCAA
NW-4	ACTGAGACGTATATTCAACGCAATGAA
NW-5	ACTGAGAGACAGATAAGCAGATAGCCGAATAGCAGCC
SW-1	AGCAAATGAAAAATCTAAAGCCTAATAGATTGTCTATGGTACCT
SW-2	ACTCACAATTTTACAACTGACGTACCT
SW-3	TGACGCTCAATCGTCTGAACTACACTGTACCT
SW-4	TCAGGGACGATATTAAACGGAGTACCT
SW-5	CCCAGTCAGGGGACGACGACAGTAGGTTTCCGTACCT
NE-1	TACGAAGGCACCAACCTAAAACCGCGACCTGCTGCATCTCAGGTA
NE-2	TGGTATAATAAGCTCGTAGTGCAGGTA
NE-3	CCAAAAGGAGCCTTTAATTCTCCCACAGGTA
NE-4	ATCAATTGTTATCCGGGTTGACAGGTA
NE-5	GGAAGGTATAATAACGGAATACGATATGCCAGGTA
NW-1b	GGCTAGTCAGAGCCGTCATTGCGGAACAAAGAAACCACC
NW-2b	GTATTGAACCAGGCTTACGCCC
NW-3b	GAATGTATGGCGAATTATTCATTTCAA
NW-4b	GACGTATATTCAACGCAATGAA
NW-5b	GAGACAGATAAGCAGATAGCCGAATAGCAGCC
SW-1b	AGCAAATGAAAAATCTAAAGCCTAATAGATTGTCTATGG
SW-2b	ACTCACAATTTTACAACTGACG
SW-3b	TGACGCTCAATCGTCTGAACTACACTG
SW-4b	TCAGGGACGATATTAAACGGAG
SW-5b	CCCAGTCAGGGGACGACGACAGTAGGTTTCCG
NE-1b	TACGAAGGCACCAACCTAAAACCGCGACCTGCTGCATCTC
NE-2b	TGGTATAATAAGCTCGTAGTGC
NE-3b	CCAAAAGGAGCCTTTAATTCTCCCAC
NE-4b	ATCAATTGTTATCCGGGTTGAC
NE-5b	GGAAGGTATAATAACGGAATACGATATGCC
SE-1b	TCTTCTCCTCCATGTTACTGTAATCTTGACAAGAACCGGA
SE-2b	TTAACGATTTGGGAGTCCAGAG
SE-3b	TCTCGCGCTAATGCAGATACATAACG
SE-4b	TGCGCTAGCTAACAAAGACGCC
SE-5b	TTCCCTTTACGTTGGTGTAGATGAAATTGT
SW-5stop	CCCAGTCAGGGGACGACGACAGTAGGTTTCCGTAC

NE-1stop	TACGAAGGCACCAACCTAAAACCGCGACCTGCTGCATCTCAGG
SE-1stop	AGTTCTTCTCCTCCATGTTACTGTAATCTTGACAAGAACCGGA
SE-5stop	AGTTTCCCTTTACGTTGGTGTAGATGAAATTGT

Table S9. Sequences of the biotinylated (cyan-colored in Figure S8), fluorophore anchoring (red-colored in Figure S8), and fluorophore modified (pink-colored in Figure S8) staple strands.

Name	Sequence
biotin-anchor-1	/5Biosg/TTTTTTTTTTATTTGGGGCGCGAGCTGTTTAGCTATATTTTCTTT
biotin-anchor-2	/5Biosg/TTTTTTTTTTAATTAGCAAAATTAAGCTAATAGTAGTAGCATTTT
biotin-anchor-3	/5Biosg/TTTTTTTTTTAACATCCAATAAATCATACAGGCAAGGCAAAGTTT
biotin-anchor-4	/5Biosg/TTTTTTTTTTAAGAAAGCGAAAGGAGCGGGCAACGGTAC
biotin-anchor-5	/5Biosg/TTTTTTTTTTTGGAACAAGAGAACGTGGCGAGAAAGGAAGGGTTT
atto-anchor-1	TTTGATTAAGACGCTGAGAACATAGCGATAGCTTATTTGAGATCCGACTACGC
atto-anchor-2	TTTGCATTCCACAGACAGCAACTACAACGCCTGTATTTGAGATCCGACTACGC
atto-anchor-3	TTTTTTGCGGGATCGTCACGGAGTTAAAGGCCGCTTTTGAGATCCGACTACGC
atto-anchor-4	TTTCTTATGCGATTTTAAGAATCATTGTGAATTACTTTGAGATCCGACTACGC
atto-anchor-5	TTTATAATCAGTGAGGCCACCTGAGAAGTGTTTTTTTTGAGATCCGACTACGC
atto-anchor-6	TTTAAACAGTTCAGAAAACCCCCCTCAAATGCTTTTTTGAGATCCGACTACGC
atto-anchor-7	TTTTTAATGCGCGAACTGAATGGCTATTAGTCTTTTGAGATCCGACTACGC
atto-anchor-8	TTTCGTAAAACAGAAATATCAAAATTATTTGCATTTGAGATCCGACTACGC
label-ATTO647N	/5ATTO647NN/AAGCGTAGTCGGATCTC

Table S10. Sequences of the photocleavable staple strands.

Name	Sequence
Adapt-NW-5-PC	GCCGGAGGATTGGCGTGGGAATCGTGCTTCTGTCTC/iSpPC/TCAGT
Adapt-NE-5-PC	TACCT/iSpPC/GGCATATCTCGCTCAGTAACTTCCCAATATGTGAGC
NW-5-HP-PC	TCAGT TTTTTT/iSpPC/ACTGAGAGACAGATAAGCAGATAGCCGAATAGCAGCC
NE-5-HP-PC	GGAAGGTATAATAACGGAATACGATATGCCAGGTA/iSpPC/TTTTTT TACCT

References

1. SantaLucia, J., Jr.; Hicks, D., The Thermodynamics of DNA Structural Motifs. *Annu. Rev. Biophys. Biomol. Struct.* **2004,** *33*, 415-440.

2. Jiang, S.; Hong, F.; Hu, H.; Yan, H.; Liu, Y., Understanding the Elementary Steps in DNA Tile-Based Self-Assembly. *ACS Nano* **2017,** *11*, 9370-9381.

3. Evans, C. G.; Hariadi, R. F.; Winfree, E., Direct Atomic Force Microscopy Observation of DNA Tile Crystal Growth at the Single-Molecule Level. *J. Am. Chem. Soc.* **2012,** *134*, 10485-10492.

4. Rothemund, P. W.; Papadakis, N.; Winfree, E., Algorithmic Self-Assembly of DNA Sierpinski Triangles. *PLoS Biol.* **2004,** *2*, e424.

5. Winfree, E. *Simulations of Computing by Self-Assembly*; CS-TR:1998.22; California Institute of Technology: Pasadena, CA, May 31, 1998.

6. Rothemund, P. W.; Ekani-Nkodo, A.; Papadakis, N.; Kumar, A.; Fygenson, D. K.; Winfree, E., Design and Characterization of Programmable DNA Nanotubes. *J. Am. Chem. Soc.* **2004,** *126*, 16344-16352.

7. Li, W.; Yang, Y.; Jiang, S.; Yan, H.; Liu, Y., Controlled Nucleation and Growth of DNA Tile Arrays within Prescribed DNA Origami Frames and Their Dynamics. *J. Am. Chem. Soc.* **2014,** *136*, 3724-3727.